

Auxiliary-Field Quantum Monte Carlo on Quantum Hardware via Unitary Dilation

Xiantao Li

*The Pennsylvania State University**

We present near-term quantum algorithms for auxiliary-field quantum Monte Carlo (AFQMC), which represents imaginary-time projection for ground-state calculation as an ensemble of one-body propagators driven by stochastic fields Ω . Starting from the Feynman-Kac formula, we convert each trajectory into a sequence of piecewise-constant one-body generators using stochastic Magnus expansions up to second order, and embed the resulting nonunitary slices into unitaries with a small ancilla overhead. This lifts the projector dynamics to a unitary evolution, enabling coherent circuit execution in the regime $\|\Omega\|\tau = \mathcal{O}(1)$ and reducing the need for frequent mid-circuit measurement. We further derive an equivalent linear-combination-of-unitaries (LCU) form that yields system-only, shallower circuits by trading ancilla cost for additional trajectory sampling. Benchmarks on the Hubbard model verify the accuracy of the dilation and Magnus expansions classically and demonstrate multi-step executions on IBM quantum hardware.

I. INTRODUCTION

Strongly correlated electronic structure is one of the most compelling applications of quantum computation. In the fault-tolerant setting, phase-estimation and qubitization based approaches, often accelerated by low-rank factorizations of the two-electron integral tensor such as tensor hypercontraction (THC), offer favorable asymptotic scaling for quantum chemistry [1–3]. However, compiled resource estimates for chemically relevant problems still require long logical runtimes and large physical-qubit overheads, well beyond current devices. In parallel, near-term variational strategies can reduce coherent circuit depth, but their accuracy depends on ansatz expressibility and the ability to optimize non-convex loss [4–6].

At the fault-tolerant level, ground-state preparation can also be achieved by spectral filtering and related imaginary-time inspired constructions, with near-optimal dependence on the spectral gap and target accuracy [7, 8]. Another important route is imaginary-time evolution (ITE), which avoids variational optimization by filtering excited-state components. Motta *et al.* introduced quantum imaginary-time evolution and quantum Lanczos as an ansatz-free framework for ground- and thermal-state preparation [9], while variational and measurement-based ITE schemes broaden the algorithmic landscape [10–12]. These methods, however, typically rely on measurement-intensive local reconstructions or variational parameter updates.

Auxiliary-field quantum Monte Carlo (AFQMC) is one of the most accurate and scalable classical methods for interacting fermionic systems, including strongly correlated materials and molecules. Through the Hubbard-Stratonovich (HS) transformation, it rewrites quartic interactions as a stochastic average over one-body propagators driven by auxiliary fields [13–18]. Because each sampled propagator maps Slater determinants (SDs) to SDs, this structure is highly attractive for quantum algorithms. Yet this structural advantage has not previ-

ously led to an explicit gate-based realization of AFQMC projector dynamics on quantum hardware. The obstacle is that each auxiliary-field slice Ω is generally nonunitary and trajectory dependent, while the projector emerges only after averaging over the trajectory ensemble. A naive implementation would therefore require either measurement-heavy adaptive updates along each trajectory or a coherent summation over trajectories with substantial postselection and depth overhead.

This work closes a critical gap by formulating the first gate-level realization of HS-driven AFQMC projector dynamics on quantum hardware, by developing a unitary dilation of nonunitary one-body propagators. The resulting slice dynamics can be executed coherently while preserving SD-to-SD structure, which can be compiled using standard Givens-rotation decompositions developed for Slater-determinant and fermionic-Gaussian state preparation [19, 20]. We construct a resource-efficient dilation primitive in the regime $\|\Omega\|\tau = \mathcal{O}(1)$, combine it with stochastic Magnus integrators for higher-order weak discretization, and derive an equivalent LCU form that yields shallower system-only circuits. In the fault-tolerant setting, we prove that the segmented construction supports coherent imaginary-time projection with linear scale-over-gap dependence and logarithmic accuracy dependence. Unlike prior hybrid AFQMC schemes, in which quantum resources are used primarily to prepare or characterize improved trial states, estimate overlap data, or reduce constraint bias while the AFQMC propagation itself remains classical [21–24], our approach implements the HS-driven projector dynamics directly as a gate-level quantum primitive. With near-term performance in mind, we use the LCU form to trade ancilla overhead for additional classical sampling and reduced circuit depth. We validate the method classically, verify the compiled circuits by statevector emulation, and demonstrate proof-of-principle multi-step executions on IBM quantum hardware.

II. METHODS AND ALGORITHMS

A. Ground-state projection and AFQMC structure

Consider an interacting N -fermion Hamiltonian in second quantization over an orthonormal spin-orbital basis, $\hat{H} = \hat{H}_1 + \hat{H}_2$, with

$$\hat{H}_1 = \sum_{ij} h_{ij} \hat{c}_i^\dagger \hat{c}_j, \quad \hat{H}_2 = \frac{1}{2} \sum_{ijkl} V_{ijkl} \hat{c}_i^\dagger \hat{c}_j^\dagger \hat{c}_l \hat{c}_k. \quad (1)$$

Given a trial state $|\psi_T\rangle$ with $\langle\psi_{\text{gs}}|\psi_T\rangle \neq 0$, imaginary-time evolution (ITE) projects onto the ground state,

$$|\psi(\tau)\rangle = e^{-\tau(\hat{H}-E_T)} |\psi_T\rangle, \quad |\psi_{\text{gs}}\rangle \propto \lim_{\tau \rightarrow \infty} |\psi(\tau)\rangle, \quad (2)$$

where E_T is an energy shift used for stabilization. In AFQMC, \hat{H}_2 is rewritten as a sum of squares of one-body operators,

$$\hat{H}_2 = -\frac{1}{2} \sum_{\gamma=1}^m \lambda_\gamma \hat{v}_\gamma^2, \quad (3)$$

with constants and one-body shifts absorbed into \hat{H}_1 and E_T . The HS transformation then converts the interacting projector into an average over one-body propagators driven by auxiliary fields. Since one-body propagators map Slater determinants (SDs) to SDs, this yields the structural foundation of AFQMC.

B. Feynman–Kac representation and stochastic differential equations (SDEs)

To avoid repeated kinetic-interaction splitting, we use a continuous-time stochastic representation of the projector. For clarity we first consider the case of real auxiliary fields, for which

$$\hat{H} = \hat{H}_1 - \sum_{\gamma=1}^m \hat{L}_\gamma^2, \quad \hat{L}_\gamma := \sqrt{\lambda_\gamma/2} \hat{v}_\gamma, \quad (4)$$

so that the scalar shift E_T contributes only an overall factor $e^{\tau E_T}$ and is omitted below. Then

$$e^{-\tau \hat{H}} = \mathbb{E} \left[\mathcal{T} e^{-\int_0^\tau \hat{H}_1 ds + \sum_{\gamma=1}^m \int_0^\tau \sqrt{2} \hat{L}_\gamma \circ dW_\gamma(s)} \right], \quad (5)$$

where $\{W_\gamma\}$ are independent Wiener processes, \circ denotes Stratonovich integration, and \mathbb{E} is expectation over Brownian paths. Equivalently, $e^{-\tau \hat{H}} |\psi_T\rangle = \mathbb{E}[|\phi_\tau\rangle]$, where $|\phi_t\rangle$ solves the Stratonovich SDE with $|\phi_0\rangle = |\psi_T\rangle$

$$d|\phi_t\rangle = \left(-\hat{H}_1 dt + \sum_{\gamma=1}^m \sqrt{2} \hat{L}_\gamma \circ dW_\gamma(t) \right) |\phi_t\rangle. \quad (6)$$

Our approach solves Eq. (6) by stochastic Magnus integrators, so that each time step is represented by a single effective one-body generator. As a result, each sampled trajectory preserves SD-to-SD structure and admits a fermionic-Gaussian circuit implementation. Despite the presence of stochastic sampling, our approach is distinct from QDrift [25], which uses randomized Hamiltonian simulation in a Trotter-style setting rather than a

stochastic representation of imaginary-time projection.

For repulsive channels one obtains instead imaginary-noise SDEs, e.g.

$$d|\phi_t\rangle = \left(-\hat{H}_1 dt + \sum_{\gamma} i\sqrt{2} \hat{K}_\gamma \circ dW_\gamma(t) \right) |\phi_t\rangle, \quad (7)$$

whose stochastic term is anti-Hermitian and generates fluctuating phases, reintroducing the usual phase problem. The general sign-indefinite Feynman–Kac representation is given in the Supplemental Material (SM).

C. Stochastic Magnus expansion

The stochastic Magnus expansion [26] expresses the one-step propagator as $U(t_{n+1}, t_n) = \exp(\Omega_n)$. Let $\Delta t = t_{n+1} - t_n$ and denote the Wiener increments $\Delta W_{\gamma,n} = W_\gamma(t_{n+1}) - W_\gamma(t_n) \sim \mathcal{N}(0, \Delta t)$. For the Stratonovich SDE (6), we write the generator in differential form as $A(t) dt = -\hat{H}_1 dt + \sum_{\gamma=1}^m \sqrt{2} \hat{L}_\gamma \circ dW_\gamma(t)$.

Weak order-1 ME. The first-order Magnus generator is $\Omega_n^{(1)} = \int_{t_n}^{t_{n+1}} A(s) ds$, yielding

$$\Omega_n^{(1)} = -\Delta t \hat{H}_1 + \sum_{\gamma=1}^m \sqrt{2} \hat{L}_\gamma \Delta W_{\gamma,n}. \quad (8)$$

Crucially, $\Omega_n^{(1)}$ is a linear combination of one-body operators, hence it maps SDs to SDs.

Weak order-2 ME. To suppress time-step errors without refining Δt , we retain the second Magnus term,

$$\Omega_n^{(2)} = \Omega_n^{(1)} + \frac{1}{2} \int_{t_n}^{t_{n+1}} \int_{t_n}^{s_1} [A(s_1), A(s_2)] ds_2 ds_1. \quad (9)$$

Substituting $dA(t)$ into the commutator produces drift-noise and noise-noise contributions. For general SDEs, the noise-noise terms generate Lévy areas and complicate higher-order schemes. Fortunately, in the density-coupled HS decomposition, widely used in lattice-based models, the diffusion operators commute, $[\hat{L}_\gamma, \hat{L}_{\gamma'}] = 0$. The only surviving second-order corrections are the drift-noise commutators $[\hat{H}_1, \hat{L}_\gamma]$, giving

$$\Omega_n^{(2)} = \Omega_n^{(1)} - \sum_{\gamma=1}^m [\hat{H}_1, \hat{L}_\gamma] J_{0\gamma,n}, \quad (10)$$

where the Stratonovich integral $J_{0\gamma,n}$ is sampled via

$J_{0\gamma,n} = \frac{\Delta t}{2} \Delta W_{\gamma,n} + \sqrt{\frac{\Delta t^3}{12}} \eta_{\gamma,n}$, $\eta_{\gamma,n} \sim \mathcal{N}(0, 1)$, (11) independent of $\Delta W_{\gamma,n}$. Because the algebra of one-body operators is closed under commutators, $[\hat{H}_1, \hat{L}_\gamma]$ remains strictly one-body, $\exp(\Omega_n^{(2)})$ can again be compiled efficiently without introducing explicit two-body gates.

D. Unitary dilation of stochastic generators

Each Magnus step produces a one-body exponent Ω_k and a generally nonunitary slice propagator e^{Ω_k} . Over one segment of duration $\tau = n_T \Delta t$, the AFQMC propagator is therefore

$$B_{\text{seg}} := e^{\Omega_{n_T}} e^{\Omega_{n_T-1}} \dots e^{\Omega_1}.$$

To implement B_{seg} coherently, we dilate each slice e^{Ω_k} and compose the resulting unitaries over the segment, so that ancilla measurement is required only once per segment rather than after every time step. General dilation schemes have been developed for both deterministic and stochastic dynamics [27]. Here we follow the moment-matching dilation framework [28, 29], and we split each slice exponent as $\Omega_k = K_k - iH_k$, with H_k and K_k Hermitian, and introduce an ancilla space \mathcal{H}_A with boundary states $\langle l|$, $|r\rangle$ and a skew-Hermitian generator F ($F^\dagger = -F$). The dilated slice Hamiltonian is

$$\tilde{H}_k = \mathbb{I}_A \otimes H_k + (iF) \otimes K_k. \quad (12)$$

Since iF and K_k are Hermitian, \tilde{H}_k is Hermitian, and the corresponding segment unitary is

$$U_{\text{seg}} := e^{-i\tilde{H}_{n_T}} e^{-i\tilde{H}_{n_T-1}} \dots e^{-i\tilde{H}_1}.$$

Projecting the ancilla then yields

$$B_{\text{seg}} \approx (\langle l| \otimes \mathbb{I}_S) U_{\text{seg}} (|r\rangle \otimes \mathbb{I}_S),$$

with a controllable postselection amplitude.

We choose iF as the nearest-neighbor hopping Hamiltonian on a 1D tight-binding chain [28]. For an n_A -qubit ancilla (dimension $d_A = 2^{n_A}$), the effective moment order scales as $m = \Theta(d_A)$, and the moment-matching error for each slice obeys

$$\left\| e^{\Omega_k} - (\langle l| \otimes \mathbb{I}) e^{-i\tilde{H}_k} (|r\rangle \otimes \mathbb{I}) \right\| = \mathcal{O}\left(\frac{\|\Omega_k\|^m}{m!}\right).$$

Thus increasing n_A suppresses the dilation error super-polynomially without increasing the system size. By contrast, first-order single-qubit-ancilla constructions based on σ_y -controlled primitives [11, 30] are intrinsically small-step, with per-slice error $\mathcal{O}(\|\Omega_n\|^2 \Delta t^2)$, and therefore require $\|\Omega_n\| \Delta t \ll 1$. By approximating the Wiener increments ΔW with a binary weak distribution [31], one obtains a bounded-support slice model and hence a uniform bound $\|\Omega_k\| \leq \|\Omega\| \Delta t$ for all admissible slices, where $\|\Omega\|$ is independent of k (see the SM). Under this bound, the postselection success remains $\Omega(1)$ provided $\|\Omega\| \tau = \mathcal{O}(1)$.

Theorem 1 (Fault-tolerant segmented imaginary-time projection). *Let \hat{H} be Hermitian with ground energy E_0 and gap $\Delta > 0$, and let $|\psi_T\rangle$ have nonzero ground overlap $\gamma > 0$. Choose $\tau = \Theta(1/\|\Omega\|)$ with $\tau = n_T \Delta t$ and $\Delta t = \Theta(\sqrt{\epsilon_{\text{prep}}})$. If the per-segment normalized preparation error is sufficiently small, namely*

$$\epsilon_{\text{prep}} = \mathcal{O}\left(\frac{(1 - e^{-2\tau\Delta})\epsilon}{\|\hat{H}\|}\right),$$

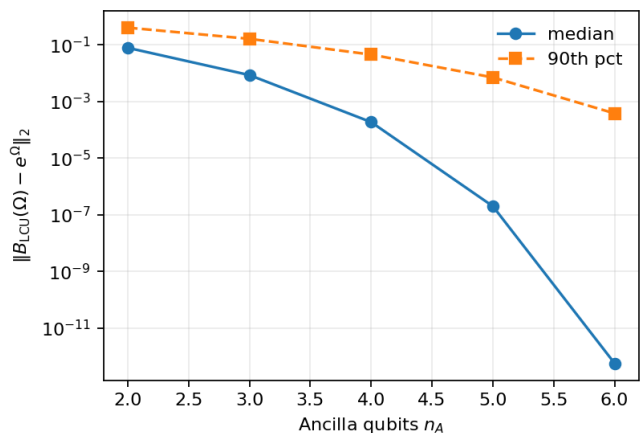


FIG. 1. One-step LCU kernel error $\|B_{\text{LCU}}(\Omega) - e^\Omega\|_2$ versus ancilla size n_A , summarized over 100 sampled weak-order-2 Magnus slice exponents Ω_k . The median and 90th percentile both decrease rapidly with n_A , showing that a modest ancilla is sufficient to make the one-step LCU approximation accurate in the constant-success regime.

then after $S = \Theta\left(\frac{\|\Omega\|}{\Delta} \log \frac{1}{\gamma\epsilon}\right)$ segments one obtains a state $|\psi_S\rangle$ with $\langle \psi_S | \hat{H} | \psi_S \rangle - E_0 \leq \epsilon$. Given a block-encoding of \hat{H}/α , the final energy can then be estimated to additive error ϵ with failure probability at most δ using $\tilde{\mathcal{O}}(\alpha \epsilon^{-1} \log(1/\delta))$ coherent queries.

In the fault-tolerant setting, the postselection amplitude can be boosted using oblivious amplitude amplification, with fixed-point variants available when robust amplification is preferred [32, 33].

Relation to prior fault-tolerant algorithms. Unlike QSP/QSVT-based ground-state filters, which treat \hat{H} through a global oracle [7, 8], Theorem 1 applies to the HS/Feynman–Kac representation and compiles the projector into coherent one-body segments. The theorem therefore matches the characteristic linear scale-over-gap segment count, $S = \Theta((\|\Omega\|/\Delta) \log \frac{1}{\gamma\epsilon})$, while the detailed per-segment implementation cost is delegated to the appendix.

The fault-tolerant construction assumes coherent segment chaining, ancilla restoration, oblivious amplitude amplification, and controlled unitaries for coherent energy estimation and trajectory superposition, which are beyond current near-term capabilities. We therefore adopt an implementable mode that keeps the same slice kernel but samples the Magnus randomness classically, while the circuit layer evaluates a small deterministic LCU over retained system-only terms. This removes coherent trajectory superposition and persistent ancilla management, yielding shallower circuits suitable for present hardware.

E. System-only implementation via LCU

A key observation is that the dilation step can be rewritten as a short linear combination of system-only unitaries by diagonalizing the ancilla generator iF . Writing

$$iF = \sum_{j=1}^{d_A} \omega_j |\chi_j\rangle\langle\chi_j|, \quad \omega_j \in \mathbb{R},$$

each slice is reduced to $U_{n,j} = e^{-i(H_n + \omega_j K_n)}$ and

$$B_{\text{seg}} = \sum_{j=1}^{d_A} c_j U_{n,j} U_{n-1,j} \cdots U_{1,j}, \quad (13)$$

where $c_j = \langle l|\chi_j\rangle\langle\chi_j|r\rangle$, up to an absorbable phase. Thus the ancilla-assisted unitary dilation of a nonunitary segment is replaced by a deterministic LCU over the retained indices j , and each term $U_{k,j}$ acts only on the system register. Since $U_{k,j}$ is generated by a quadratic fermionic Hamiltonian, it can be compiled as a fermionic Gaussian circuit, substantially reducing the two-qubit depth relative to a direct dilation circuit for the combined dilated Hamiltonian \tilde{H} . For near-term implementations, the Magnus randomness is sampled classically as in AFQMC, while the LCU over j is evaluated deterministically. This removes the dilation register from the executed circuit and trades ancilla overhead for additional classical preprocessing and a moderate increase in the number of measured system-only circuits. Moreover, because each $U_{k,j}$ is a quadratic-fermion propagator, it is compiled directly as a fermionic Gaussian circuit rather than through an additional Trotter decomposition, which further helps control circuit depth. This passage from dilation to an LCU of system-only Hamiltonian simulations is analogous to the relation between Schrödingerization [27] and LCHS [34].

In the near-term mode, the sampling overhead grows linearly with the number of classical trajectories N_{traj} , the number r of LCU terms, and the number N_{obs} of observables entering the mixed estimator. For a fixed shot budget per circuit, this gives a total measurement cost proportional to $N_{\text{traj}} r N_{\text{obs}}$. For a system with n_{orb} spin-orbitals, each retained segment unitary is a quadratic-fermion propagator and can be compiled directly as a fermionic Gaussian circuit using $\mathcal{O}(n_{\text{orb}}^2)$ Givens rotations, avoiding an additional Trotter decomposition and helping keep the coherent depth low on near-term hardware.

III. NUMERICAL TEST

We benchmark the stochastic Magnus+dilation/LCU construction on the half-filled two-site Hubbard dimer in a four-spin-orbital Jordan–Wigner encoding, initialized from the Hartree–Fock determinant [100]. The code

uses $t = 1$, $U = 4$, and the particle-hole-shifted interaction $U \sum_i (n_{i\uparrow} - \frac{1}{2})(n_{i\downarrow} - \frac{1}{2})$. Classical checks use sampled AFQMC trajectories, while the hardware study uses mixed estimators built from compiled LCU circuits. To reduce circuit depth, the circuit synthesis uses the re-ordered orbital basis $(1 \uparrow, 2 \uparrow, 1 \downarrow, 2 \downarrow)$, for which the one-body propagator is spin-block diagonal.

We first examine the LCU kernel itself. Figure 1 shows the one-step LCU approximation error as a function of ancilla size. Over sampled weak-order-2 Magnus slice exponents, the median error drops rapidly with n_A , reaching the 10^{-3} level already for $n_A = 3-4$, while the 90th-percentile error decreases substantially as well. This rapid convergence shows that only a modest ancilla is needed to control the per-slice LCU approximation in the constant-success regime, and it provides a practical guideline for choosing n_A in the later simulations.

We next validate the stochastic Magnus propagation at the classical level. Figure 2 compares AFQMC energies obtained from unitary dilations of the first- and second-order Magnus discretizations against deterministic imaginary-time references from $\exp(-\tau \hat{H})$. For larger step sizes, the second-order scheme follows both the mixed-estimator and Rayleigh-quotient references more closely over $\tau \leq 0.3$, while the first-order scheme shows a visibly larger time-discretization bias. Thus the pathwise propagation captures the intended imaginary-time relaxation, and the weak-order improvement translates directly into more accurate physical observables.

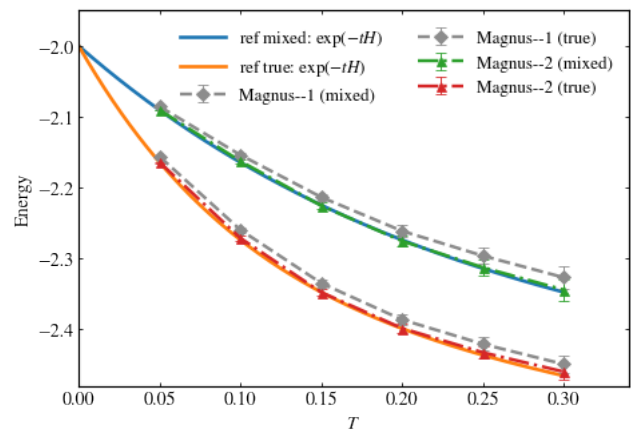


FIG. 2. Energy estimates versus imaginary time T comparing Magnus-1 and Magnus-2 AFQMC propagation. Dashed and dash-dot curves with markers show mixed and true (Rayleigh) estimators with jackknife error bars, and solid lines denote the corresponding $\exp(-\tau \hat{H})$ references.

We then test segmented propagation. Figure 3 compares the two-segment ME-2 dilation simulation with the deterministic imaginary-time reference. The mixed estimator closely follows the corresponding mixed-reference curve, while the exact estimator remains consistent with

the Rayleigh quotient, showing that the propagated ensemble continues to approximate the intended projected state after segment chaining. The absence of an observable kink at the segment boundary indicates that the segment-wise collapse/reset preserves continuity and enables accurate multi-segment evolution up to $T \simeq 0.6$ in this benchmark.

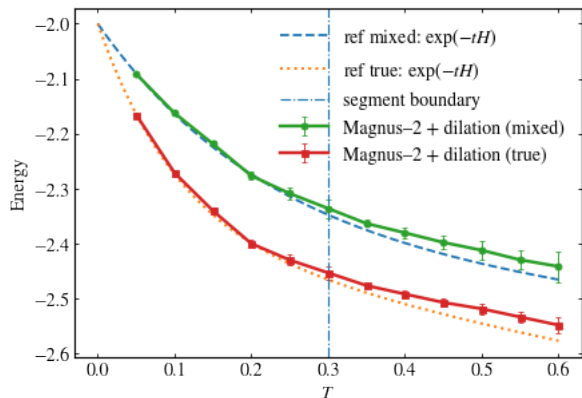


FIG. 3. Energy estimates versus imaginary time τ for the two-segment Magnus-2 dilation simulation. Circles (squares) show the mixed (true/Rayleigh) estimator with path-sampling error bars; dashed (dotted) curves denote the corresponding deterministic references computed from $\exp(-\tau\hat{H})$. The vertical dash-dot line marks the segment boundary.

Finally, we assess the near-term viability of the LCU implementation on IBM-Boston. We use the trial state $|\psi_T\rangle$ as the reference state in the mixed estimator, sample $n_{\text{traj}} = 40$ trajectories, and use 400 shots per circuit. For each trajectory, the AFQMC segment map is compiled as a fermionic Gaussian circuit via Givens rotations. The hardware runs use IBM Runtime error-suppression and mitigation options, including resilience level 1 and dynamical decoupling. The resulting circuits use 5 logical qubits and transpile to 7 active physical qubits, with median depth 271 and median two-qubit count 77 CZ gates on IBM-Boston.

Figure 4 compares the exact mixed estimator, the statevector emulation of the compiled circuits, and the IBM hardware data as a function of the number of Magnus steps n_T . The statevector emulator follows the exact mixed-estimator trend qualitatively, indicating that the compiled circuits retain the intended imaginary-time projection signal. The IBM data remain in the same energy window and are statistically consistent with the simulator at the proof-of-principle level, although with substantially larger uncertainties. We expect that the remaining discrepancy can be reduced by increasing n_A to suppress the dilation error without increasing circuit depth, by using more accurate error-mitigation protocols, and by executing the circuits on hardware with lower physical

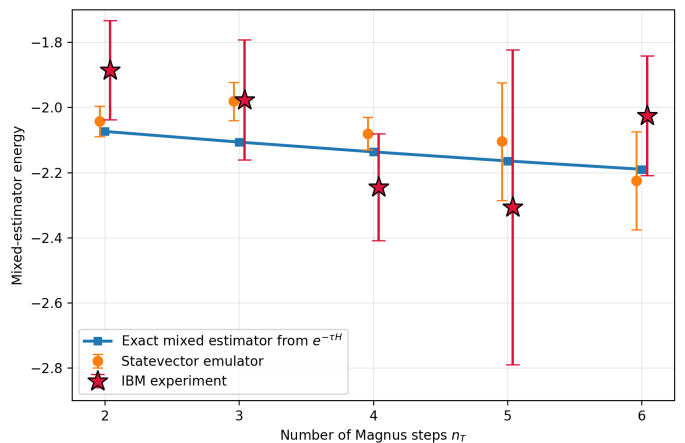


FIG. 4. Mixed-estimator energies versus the number of Magnus steps n_T . Blue squares denote the exact mixed estimator $\langle\psi_T|He^{-\tau H}|\psi_T\rangle/\langle\psi_T|e^{-\tau H}|\psi_T\rangle$, orange circles the statevector emulation of the compiled LCU circuits, and red stars the IBM-Boston hardware results. Error bars show bootstrap standard errors for the emulator and hardware data.

error rates.

IV. SUMMARY AND DISCUSSION

We introduced a quantum-native AFQMC framework in which HS projector dynamics is discretized by stochastic Magnus slices and each nonunitary one-body step is implemented by dilation or LCU, preserving Slater-to-Slater structure and yielding hardware-executable fermionic-Gaussian circuits. In this formulation, the sign/phase problem appears directly as an algorithmic resource through the success probability, effective ℓ_1 weight, and estimator variance, suggesting extensions that combine constrained-path or phaseless controls with quantum-assisted overlap estimation and importance sampling [18, 35, 36]. Another promising direction is finite-temperature and thermal-state simulation, where the same HS-based compiler may be extended beyond ground-state projection [9, 12]. More broadly, these results point to a new interface between AFQMC and quantum hardware, while leaving open the central question of whether quantum resources can mitigate the practical severity of sign/phase bottlenecks despite their worst-case hardness [35].

Acknowledgements. – This work was supported by NSF Grant No. DMS-2411120. This research used resources of the National Energy Research Scientific Computing Center (NERSC), a Department of Energy Office of Science User Facility under Contract No. DE-AC02-05CH11231 using NERSC award DDR-ERCAP0035683.

-
- * Xiantao.Li@psu.edu
- [1] R. Babbush, C. Gidney, D. W. Berry, N. Wiebe, J. McClean, A. Paler, A. Fowler, and H. Neven, *Phys. Rev. X* **8**, 041015 (2018).
 - [2] J. Lee, D. W. Berry, C. Gidney, M. Motta, J. R. McClean, and R. Babbush, *PRX Quantum* **2**, 030305 (2021).
 - [3] B. Bauer, S. Bravyi, M. Motta, and G. K.-L. Chan, *Chem. Rev.* **120**, 12685 (2020).
 - [4] A. Peruzzo, J. McClean, P. Shadbolt, M.-H. Yung, X.-Q. Zhou, P. J. Love, A. Aspuru-Guzik, and J. L. O'Brien, *Nat. Commun.* **5**, 4213 (2014).
 - [5] A. Kandala, A. Mezzacapo, K. Temme, M. Takita, M. Brink, J. M. Chow, and J. M. Gambetta, *Nature* **549**, 242 (2017).
 - [6] J. R. McClean, J. Romero, R. Babbush, and A. Aspuru-Guzik, *New Journal of Physics* **18**, 023023 (2016), arXiv:1509.04279 [quant-ph].
 - [7] L. Lin and Y. Tong, *Quantum* **4**, 372 (2020), arXiv:2002.12508 [quant-ph].
 - [8] Y. Dong, L. Lin, and Y. Tong, *PRX Quantum* **3**, 040305 (2022), arXiv:2204.05955 [quant-ph].
 - [9] M. Motta, C. Sun, A. T. K. Tan, M. J. O'Rourke, E. Ye, A. J. Minnich, F. G. S. L. Brandão, and G. K.-L. Chan, *Nature Physics* **16**, 205 (2020).
 - [10] S. McArdle, T. Jones, S. Endo, Y. Li, S. C. Benjamin, and X. Yuan, *npj Quantum Inf.* **5**, 75 (2019).
 - [11] Y. Mao, M. Chaudhary, M. Kondappan, J. Shi, E. O. Ilo-Okeke, V. Ivannikov, and T. Byrnes, *Physical Review Letters* **131**, 110602 (2023).
 - [12] S.-N. Sun, M. Motta, R. N. Tazhigulov, A. T. K. Tan, G. K.-L. Chan, and A. J. Minnich, *PRX Quantum* **2**, 010317 (2021).
 - [13] J. Hubbard, *Phys. Rev. Lett.* **3**, 77 (1959).
 - [14] R. L. Stratonovich, *Sov. Phys. Dokl.* **2**, 416 (1958).
 - [15] J. E. Hirsch, *Phys. Rev. B* **28**, 4059 (1983).
 - [16] S. Zhang, J. Carlson, and J. E. Gubernatis, *Phys. Rev. B* **55**, 7464 (1997).
 - [17] M. Motta, S. Zhang, and G. K.-L. Chan, *Physical Review B* **100**, 045127 (2019), arXiv:1905.00511 [physics.comp-ph].
 - [18] H. Shi and S. Zhang, *J. Chem. Phys.* **154**, 024107 (2021).
 - [19] Z. Jiang, K. J. Sung, K. Kechedzhi, V. N. Smelyanskiy, and S. Boixo, *Physical Review Applied* **9**, 044036 (2018), arXiv:1711.05395 [quant-ph].
 - [20] I. D. Kivlichan, J. McClean, N. Wiebe, C. Gidney, A. Aspuru-Guzik, G. K.-L. Chan, and R. Babbush, *Physical Review Letters* **120**, 110501 (2018), arXiv:1711.04789 [quant-ph].
 - [21] W. J. Huggins, B. A. O'Gorman, N. C. Rubin, D. R. Reichman, R. Babbush, and J. Lee, *Nature* **603**, 416 (2022).
 - [22] M. Amsler, P. Deglmann, M. Degroote, M. P. Kaicher, M. Kiser, M. Kühn, C. Kumar, A. Maier, G. Samsonidze, A. Schroeder, M. Streif, D. Vodola, and C. Wever, *The Journal of Chemical Physics* **159**, 044119 (2023).
 - [23] B. Huang, Y.-T. Chen, B. Gupt, M. Suchara, A. Tran, S. McArdle, and G. Galli, *Physical Review Research* **6**, 043063 (2024).
 - [24] D. Danilov, J. Robledo-Moreno, K. J. Sung, M. Motta, and J. Shee, arXiv preprint arXiv:2503.05967 (2025), arXiv:2503.05967 [quant-ph].
 - [25] E. Campbell, *Phys. Rev. Lett.* **123**, 070503 (2019).
 - [26] K. Kamm, S. Pagliarani, and A. Pascucci, *Journal of Scientific Computing* **89**, 56 (2021).
 - [27] S. Jin, N. Liu, and Y. Yu, *Phys. Rev. Lett.* **133**, 230602 (2024).
 - [28] X. Li, arXiv preprint arXiv:2507.10285 (2025).
 - [29] H.-C. Wu and X. Li, arXiv preprint arXiv:2601.05928 (2026).
 - [30] T. Liu, J.-G. Liu, and H. Fan, *Quantum Information Processing* **20**, 204 (2021).
 - [31] P. E. Kloeden and E. Platen, *Numerical solution of stochastic differential equations* (Springer, 1992).
 - [32] D. W. Berry, A. M. Childs, R. Cleve, R. Kothari, and R. D. Somma, *Physical Review Letters* **114**, 090502 (2015).
 - [33] T. J. Yoder, G. H. Low, and I. L. Chuang, *Physical Review Letters* **113**, 210501 (2014), arXiv:1409.3305 [quant-ph].
 - [34] D. An, J.-P. Liu, and L. Lin, *Physical Review Letters* **131**, 150603 (2023), arXiv:2303.01029.
 - [35] M. Troyer and U.-J. Wiese, *Phys. Rev. Lett.* **94**, 170201 (2005).
 - [36] S. Zhang and H. Krakauer, *Phys. Rev. Lett.* **90**, 136401 (2003).
 - [37] P. Rall, *Quantum* **5**, 491 (2021).

Auxiliary-Field Quantum Monte Carlo on Quantum Hardware via Unitary Dilation.

Appendix A: The moment-fulfilling dilation method

Suppose we are simulating a non-unitary evolution with generator Ω with both H and K being Hermitian. Our moment-fulfilling framework is built on the projected dilated propagator

$$\langle l| \otimes I \rangle e^{-it\tilde{H}} (|r\rangle \otimes I), \quad \tilde{H} := I \otimes H + (iF) \otimes K, \quad (\text{A1})$$

which recovers the target non-unitary evolution exactly when the moment identities

$$\langle l|F^k|r\rangle = 1, \quad \forall k \geq 0,$$

hold. The proof is algebraic [28]: expand the unitary $e^{-it\tilde{H}}$ (or its time-ordered Dyson series) and use the moment identities to collapse every occurrence of F^k inside the matrix element, thereby reproducing the Taylor/Dyson series of $e^{t(-iH+K)}$ term-by-term.

In the finite-dimensional tight-binding realization used here, F is approximated by the skew-Hermitian chain θF_h on grid points $p_j = jh$ with $h = 1/M$ and the trapezoid-weight. When $\theta = 2$, we have

$$\begin{aligned} (F_h \mathbf{v})_0 &= \frac{1}{2\sqrt{2}} v_1, \\ (F_h \mathbf{v})_1 &= \frac{3}{4} v_2 - \frac{1}{2\sqrt{2}} v_0, \\ (F_h \mathbf{v})_i &= \frac{p_{i+1} + p_i}{4h} v_{i+1} - \frac{p_i + p_{i-1}}{4h} v_{i-1}, \quad 2 \leq i \leq M-1, \\ (F_h \mathbf{v})_M &= -\frac{p_{M-1} + p_M}{4h} v_{M-1}. \end{aligned} \quad (\text{A2})$$

In addition, the vector $|r_h\rangle$ is given by,

$$|r_h\rangle = \frac{h}{2} |0\rangle + h \sum_{i=1}^{M-1} |i\rangle + \frac{h}{2} |M\rangle. \quad (\text{A3})$$

When implemented with an ancilla register, we choose $n_A = \log_2(M+1)$.

A key property is that $|r_h\rangle$ is an *interior* eigenmode of θF_h up to a rank-one defect at the right boundary:

$$(\theta F_h) |r_h\rangle - |r_h\rangle = \alpha |M\rangle, \quad (\text{A4})$$

for some scalar α [28]. Equivalently, the residual vanishes on all interior nodes $j < M$ and is supported only at the terminal site $|M\rangle$.

The dilated evolution in (A1) will be followed by post-selection to reduce the system register to follow the non-unitary evolution. Let Π_{win} denote projection onto a prefront window that excludes the boundary, e.g.

$$\Pi_{\text{win}} = \sum_{j=0}^{j^*} |j\rangle\langle j|, \quad j^* = \frac{M}{2}.$$

Because F_h is nearest-neighbor on the ancilla chain, any component injected at $|M\rangle$ can propagate left by at most one site per application of F_h . Consequently, for every $k \leq m := M - j^*$ the boundary defect in (A4) cannot reach the window, and we have the *windowed moment identities*

$$\Pi_{\text{win}} (\theta F_h)^k |r_h\rangle = \Pi_{\text{win}} |r_h\rangle, \quad \text{hence} \quad \langle l_h | (\theta F_h)^k |r_h\rangle = 1, \quad k = 0, 1, \dots, m, \quad (\text{A5})$$

where $\langle l_h |$ is any evaluation functional supported inside the window,

$$\langle l_h | = \frac{\sum_{i=0}^{j^*} \langle i |}{\sum_{i=0}^{j^*} \langle i |r_h\rangle}. \quad (\text{A6})$$

Together, Eqs. (A2), (A3) and (A6) constitute the elements needed to apply the dilation scheme (A1).

Define the target slice map $B(t) := e^{t(-iH+K)}$, and let $\tilde{B}(t)$ be the windowed dilation kernel obtained by applying $\langle l_h | \otimes I$ and $(|r_h\rangle \otimes I)$ together with the window projection Π_{win} . Expanding both $B(t)$ and $\tilde{B}(t)$ in Taylor series, the finite moment identities (A5) imply that the two series *agree through order m*. Therefore the mismatch is controlled by the Taylor remainder:

$$\|B(t) - \tilde{B}(t)\| \leq \sum_{k=m+1}^{\infty} \frac{(t\|\Omega\|)^k}{k!} \leq \frac{(t\|\Omega\|)^{m+1}}{(m+1)!} e^{t\|\Omega\|}, \quad (\text{A7})$$

and in the constant-success regime where $t\|\Omega\| = \mathcal{O}(1)$ this simplifies to the advertised factorial scaling

$$\|B(t) - \tilde{B}(t)\| \lesssim \frac{(t\|\Omega\|)^{m+1}}{(m+1)!}.$$

With the symmetric choice $j^* = M/2$ (so $m = M/2$), we obtain

$$\|B(t) - \tilde{B}(t)\| \lesssim \frac{(t\|\Omega\|)^{M/2+1}}{(M/2+1)!},$$

which is the finite-moment analogue of the exact all-orders recovery in the infinite-dimensional moment-matching dilation. For the time-dependent case $H(t), K(t)$, this procedure can be applied with Dyson series expansions [28].

Appendix B: The Derivation of the operator bound for HS/Magnus slices

Our dilation primitive operates in a constant-success/window regime when the segment length τ satisfies $\tau K_{\max} = \mathcal{O}(1)$, where $K_{\max} := \max_{t \in [0, \tau]} \|K(t)\|$ (or $K_{\max} := \max_n \|K_n\|$ in a discrete-time implementation) [28]. A sufficient condition is the explicit bound $\tau \leq (e\theta K_{\max})^{-1}$ [28].

Consider the Stratonovich SDE in the Feynman-Kac formula

$$d|\phi_t\rangle = \left(-\hat{H}_1 dt + \sum_{\gamma=1}^m \sqrt{2} \hat{L}_\gamma \circ dW_\gamma(t) \right) |\phi_t\rangle,$$

and the associated one-step Magnus exponent Ω_n over $[t_n, t_{n+1}]$.

For weak order 1,

$$\Omega_n^{(1)} = -\Delta t \hat{H}_1 + \sum_{\gamma=1}^m \sqrt{2} \hat{L}_\gamma \Delta W_{\gamma,n},$$

which is Hermitian when $\hat{H}_1, \hat{L}_\gamma$ are Hermitian and $\Delta W_{\gamma,n} \in \mathbb{R}$. For weak order 2 with commuting diffusion fields, a correction term appears

$$\Omega_n^{(2)} = \Omega_n^{(1)} - \sum_{\gamma=1}^m [\hat{H}_1, \hat{L}_\gamma] J_{0\gamma,n}.$$

Since $[\hat{H}_1, \hat{L}_\gamma]$ is skew-Hermitian and $J_{0\gamma,n} \in \mathbb{R}$, the second-order term is purely skew-Hermitian and therefore does not change the Hermitian part, K_n , of Ω_n . Hence Magnus-1 and Magnus-2 have the same contractive component:

$$K_n := -\Delta t \hat{H}_1 + \sum_{\gamma=1}^m \sqrt{2} \hat{L}_\gamma \Delta W_{\gamma,n}.$$

By the triangle inequality,

$$\|K_n\| \leq \Delta t \|\hat{H}_1\| + \sum_{\gamma=1}^m \sqrt{2} \|\hat{L}_\gamma\| |\Delta W_{\gamma,n}|.$$

If we implement $\Delta W_{\gamma,n}$ via a bounded Hutchinson/Rademacher approximation [31] $\Delta W_{\gamma,n} = \sqrt{\Delta t} \xi_{\gamma,n}$ with $|\xi_{\gamma,n}| \leq \sqrt{3}$, then a pathwise uniform bound is found,

$$\|K_n\| \leq \Delta t \|\hat{H}_1\| + \sqrt{6\Delta t} \sum_{\gamma=1}^m \|\hat{L}_\gamma\|.$$

This provides an explicit bound that determines the time interval to which the dilation method can be applied with constant success. For example, for weak order 1 scheme applied until $t = 1$, we should have

$$\|\Omega\| := \left\| \Omega_n^{(1)} \right\| / \Delta t \leq \|\hat{H}_1\| + \sqrt{6/\Delta t} \sum_{\gamma=1}^m \|\hat{L}_\gamma\|.$$

Appendix C: LCU coefficient normalization and constant success

We recall the discrete spectral decomposition of the ancilla generator and the resulting LCU form. Let $F_h = -i \sum_{j=0}^M \omega_j |\phi_j\rangle\langle\phi_j|$ with $\omega_j \in \mathbb{R}$ and $\{|\phi_j\rangle\}$ orthonormal. Then the dilated propagator factorizes in this eigenbasis

and yields a system-only expansion

$$B(t) = \sum_{j=0}^M c_j U_j(t), \quad U_j(t) := \mathcal{T} \exp\left(-i \int_0^t (H(s) + \omega_j K(s)) ds\right), \quad (\text{C1})$$

with coefficients

$$c_j := \langle l_h | \phi_j \rangle \langle \phi_j | r_h \rangle. \quad (\text{C2})$$

Here $(\langle l_h |, |r_h \rangle)$ are the windowed boundary vectors. For the window $\text{win} = \{0, 1, \dots, j^*\}$, define the window weight

$$P_{\text{win}} := \sum_{j \in \text{win}} |\langle j | r_h \rangle|^2 = \|\Pi_{\text{win}} |r_h \rangle\|^2, \quad \Pi_{\text{win}} := \sum_{j \in \text{win}} |j \rangle \langle j|. \quad (\text{C3})$$

In the constant-success regime (segment length $t\|K\| = \mathcal{O}(1)$ with windowed readout), $P_{\text{win}} = \Omega(1)$.

Lemma 2 (ℓ_1 -bound for the LCU coefficients). *With c_j defined in (C2), one has*

$$\|c\|_1 := \sum_{j=0}^M |c_j| \leq \|l_h\| \|r_h\|. \quad (\text{C4})$$

In particular, for the dilation-consistent normalization used in (C1) one may take $\|r_h\| = 1$ and $\|l_h\| = 1/\sqrt{P_{\text{win}}}$, hence

$$\|c\|_1 \leq \frac{1}{\sqrt{P_{\text{win}}}} = \mathcal{O}(1). \quad (\text{C5})$$

Proof. By (C2) and Cauchy–Schwarz,

$$\sum_{j=0}^M |c_j| = \sum_{j=0}^M |\langle l_h | \phi_j \rangle \langle \phi_j | r_h \rangle| \leq \left(\sum_{j=0}^M |\langle l_h | \phi_j \rangle|^2 \right)^{1/2} \left(\sum_{j=0}^M |\langle \phi_j | r_h \rangle|^2 \right)^{1/2}.$$

Since $\{\phi_j\}$ is an orthonormal basis, the two sums are $\|l_h\|^2$ and $\|r_h\|^2$, proving (C4). For the windowed/truncated choice, $\|r_h\|$ is normalized to 1 and l_h carries the window renormalization $\|l_h\| = 1/\|\Pi_{\text{win}} r_h\| = 1/\sqrt{P_{\text{win}}}$, which gives (C5). \square

Appendix D: Extension to general two-body decompositions with both signs

Our numerical tests have considered attractive two-body interactions. In general, after normal ordering and a square decomposition of the interaction kernel, e.g., by diagonalization or Cholesky factorization, followed if needed by a Hermitian recombination of channels, the two-body part can be written as

$$\hat{H}_2 = \frac{1}{2} \sum_{\gamma=1}^m \lambda_\gamma \hat{v}_\gamma^2 + \hat{H}_{\text{shift}}, \quad (\text{D1})$$

where each \hat{v}_γ is one-body, i.e., quadratic in fermionic creation/annihilation operators, $\lambda_\gamma \in \mathbb{R}$ may have either sign, and \hat{H}_{shift} collects constant and one-body terms that can be absorbed into \hat{H}_1 and the energy offset [17, 18].

For $\lambda_\gamma < 0$, the Hubbard–Stratonovich (HS) transformation introduces a real auxiliary field,

$$e^{-(\tau/2)\lambda_\gamma \hat{v}_\gamma^2} = \frac{1}{\sqrt{2\pi}} \int_{\mathbb{R}} dx_\gamma e^{-x_\gamma^2/2} \exp(x_\gamma \sqrt{-\tau\lambda_\gamma} \hat{v}_\gamma), \quad (\text{D2})$$

so each sample contributes a generally nonunitary one-body factor $\exp(\eta_\gamma \hat{v}_\gamma)$ with real η_γ . This is the case emphasized in the main text, where each slice is implemented by dilation or LCU.

For $\lambda_\gamma > 0$, the HS coupling is imaginary,

$$e^{-(\tau/2)\lambda_\gamma \hat{v}_\gamma^2} = \frac{1}{\sqrt{2\pi}} \int_{\mathbb{R}} dx_\gamma e^{-x_\gamma^2/2} \exp(i x_\gamma \sqrt{\tau\lambda_\gamma} \hat{v}_\gamma). \quad (\text{D3})$$

If \hat{v}_γ is Hermitian, the sampled noise factor is unitary. The full imaginary-time slice is still nonunitary because of the deterministic drift, and the Monte Carlo estimator acquires fluctuating complex phases, i.e., the usual phase problem [16, 18, 36].

Rather than HS transformation, this paper relies on the Feynman-Kac formula. Let

$$\hat{H} = \hat{H}_1 + \frac{1}{2} \sum_{\gamma=1}^m \lambda_\gamma \hat{v}_\gamma^2 + \hat{H}_{\text{shift}}, \quad (\text{D4})$$

and let $\{W_\gamma(\tau)\}_{\gamma=1}^m$ be independent standard real Wiener processes. Define

$$\sigma_\gamma := \begin{cases} \sqrt{-\lambda_\gamma}, & \lambda_\gamma < 0, \\ i\sqrt{\lambda_\gamma}, & \lambda_\gamma > 0, \end{cases} \quad \text{so that} \quad \sigma_\gamma^2 = -\lambda_\gamma. \quad (\text{D5})$$

Then the propagator-valued process $\hat{B}(\tau)$ may be defined in Stratonovich form by

$$d\hat{B}(\tau) = -(\hat{H}_1 + \hat{H}_{\text{shift}})\hat{B}(\tau) d\tau + \sum_{\gamma=1}^m \sigma_\gamma \hat{v}_\gamma \hat{B}(\tau) \circ dW_\gamma(\tau), \quad \hat{B}(0) = \mathbb{I}. \quad (\text{D6})$$

Pathwise, $\hat{B}(\tau)$ is the time-ordered stochastic exponential

$$\hat{B}(\tau) = \mathcal{T} \exp\left(-\int_0^\tau (\hat{H}_1 + \hat{H}_{\text{shift}}) ds + \sum_{\gamma=1}^m \int_0^\tau \sigma_\gamma \hat{v}_\gamma \circ dW_\gamma(s)\right), \quad (\text{D7})$$

and its expectation satisfies

$$\mathbb{E}[\hat{B}(\tau)] = e^{-\tau \hat{H}}. \quad (\text{D8})$$

Thus the same stochastic representation covers both attractive and repulsive channels in one framework. When $\lambda_\gamma < 0$, the noise factors are generally nonunitary. When $\lambda_\gamma > 0$ and \hat{v}_γ is Hermitian, the noise factors are unitary but the estimator becomes oscillatory because of complex phases. This is precisely the setting in which constrained-path or phaseless controls are introduced in classical AFQMC [16, 18, 36].

Appendix E: Extensions to higher-order stochastic Magnus terms

We have mainly considered the first- and second-order Magnus expansion in the paper. This expansion can be continued to include higher-order stochastic integrals [26, 31], and thus leads to more accurate stochastic paths.

Let $U(t_{n+1}, t_n) = \exp(\Omega_n)$ denote the one-step propagator, with stochastic differential generator written in Stratonovich form as

$$A(t) dt = -\hat{H}_1 dt + \sqrt{2} \sum_{\gamma=1}^m \hat{v}_\gamma \circ dW_\gamma(t).$$

Formally,

$$U(t_{n+1}, t_n) = \mathcal{T} \exp\left(\int_{t_n}^{t_{n+1}} A(s)\right), \quad \Omega_n = \Omega_{n,1} + \Omega_{n,2} + \Omega_{n,3} + \Omega_{n,4} + \dots$$

The first three Magnus terms have the standard commutator form

$$\Omega_{n,1} = \int_{t_n}^{t_{n+1}} A(s_1), \quad (\text{E1})$$

$$\Omega_{n,2} = \frac{1}{2} \int_{t_n}^{t_{n+1}} \int_{t_n}^{s_1} [A(s_1), A(s_2)], \quad (\text{E2})$$

$$\Omega_{n,3} = \frac{1}{6} \int_{t_n}^{t_{n+1}} \int_{t_n}^{s_1} \int_{t_n}^{s_2} \left([A(s_1), [A(s_2), A(s_3)]] + [A(s_3), [A(s_2), A(s_1)]]\right), \quad (\text{E3})$$

and $\Omega_{n,4}$ is the corresponding fourth-order nested-commutator term [26]. In the Stratonovich setting these expressions have the same formal structure as in the deterministic Magnus expansion, except that the coefficients are iterated Stratonovich stochastic integrals.

For the density-coupled HS decomposition used in the main text, the diffusion operators commute,

$$[\hat{v}_\gamma, \hat{v}_{\gamma'}] = 0 \quad \forall \gamma, \gamma'.$$

Hence all pure noise-noise commutator terms vanish. At second order this removes Lévy-area contributions and yields the order-2 generator in the paper. At higher orders, the only Lie brackets that can appear are nested commutators involving \hat{H}_1 and the \hat{v}_γ , for example

$$[\hat{H}_1, \hat{v}_\gamma], \quad [\hat{H}_1, [\hat{H}_1, \hat{v}_\gamma]], \quad [\hat{v}_{\gamma'}, [\hat{H}_1, \hat{v}_\gamma]], \dots$$

All of these remain one-body because commutators of one-body fermionic operators are one-body. Therefore the third- and fourth-order Magnus truncations,

$$\Omega_n^{(3)} := \Omega_{n,1} + \Omega_{n,2} + \Omega_{n,3}, \quad \Omega_n^{(4)} := \Omega_n^{(3)} + \Omega_{n,4},$$

still generate fermionic Gaussian maps $\exp(\Omega_n^{(3)})$ and $\exp(\Omega_n^{(4)})$ that preserve Slater-determinant structure.

In the commuting-noise setting, the additional random variables entering higher-order Magnus truncations can be expressed in terms of a small number of time-integrated Brownian functionals per channel, in addition to the Wiener increment

$$\Delta W_{\gamma,n} = W_\gamma(t_{n+1}) - W_\gamma(t_n) \sim \mathcal{N}(0, \Delta t).$$

For example, on a single step $[0, \Delta t]$, they are given by,

$$J_{0\gamma} := \int_0^{\Delta t} W_\gamma(s) ds = \int_0^{\Delta t} (\Delta t - s) dW_\gamma(s), \quad (\text{E4})$$

$$J_{00\gamma} := \int_0^{\Delta t} \int_0^{s_1} W_\gamma(s_2) ds_2 ds_1 = \int_0^{\Delta t} \frac{(\Delta t - s)^2}{2} dW_\gamma(s), \quad (\text{E5})$$

$$J_{000\gamma} := \int_0^{\Delta t} \int_0^{s_1} \int_0^{s_2} W_\gamma(s_3) ds_3 ds_2 ds_1 = \int_0^{\Delta t} \frac{(\Delta t - s)^3}{6} dW_\gamma(s). \quad (\text{E6})$$

These variables are linear functionals of the Brownian path and therefore are jointly Gaussian with $\Delta W_{\gamma,n}$. Their covariance matrix is obtained directly from the Itô-integral representations above via Itô isometry [31]. Thus higher-order Magnus sampling requires only a modest Gaussian preprocessing layer, while the quantum step remains the implementation of a one-body exponential.

When the diffusion operators do not commute, the second-order Magnus correction additionally involves Lévy-area terms. However, these enter through commutators of one-body operators and therefore still produce an effective one-body generator, so a weak second-order method remains implementable within the same fermionic-Gaussian framework.

Appendix F: Proof of the main Theorem

Theorem 3. *Let \hat{H} be Hermitian with eigenvalues $E_0 < E_1 \leq \dots$, gap $\Delta := E_1 - E_0 > 0$, and eigenvectors $|E_0\rangle, |E_1\rangle, \dots$. Let $|\psi_T\rangle$ be a normalized trial wave function with ground overlap $\gamma := |\langle E_0 | \psi_T \rangle|^2 > 0$, and define*

$$|\psi(\tau)\rangle := \frac{e^{-\tau(\hat{H}-E_T)} |\psi_T\rangle}{\|e^{-\tau(\hat{H}-E_T)} |\psi_T\rangle\|}, \quad E_T \in \mathbb{R}.$$

We choose a path-independent Magnus bound as in Section B

$$\|\Omega_n(\omega)\| \leq \|\Omega\| \Delta t,$$

and a segment length $\tau = n_T \Delta t$ with

$$\tau = \Theta(1/\|\Omega\|), \quad \Delta t = \Theta(\sqrt{\epsilon_{\text{prep}}}). \quad (\text{F1})$$

Assume further that one segment admits a coherent fault-tolerant implementation of the normalized update map with uniform state-preparation error

$$\sup_{\rho} \|\tilde{\Phi}_\tau(\rho) - \Phi_\tau(\rho)\|_1 \leq c_{\text{prep}} \epsilon_{\text{prep}},$$

where

$$\Phi_\tau(\rho) = \frac{K_\tau \rho K_\tau}{\text{Tr}(K_\tau \rho K_\tau)}, \quad K_\tau = e^{-\tau(\hat{H}-E_T)}.$$

Then there is a fault-tolerant algorithm that, after

$$S = \Theta\left(\kappa \log \frac{1}{\gamma \epsilon}\right), \quad \kappa := \frac{\|\Omega\|}{\Delta},$$

segments, prepares a normalized state $|\psi_S\rangle$ satisfying

$$\langle \psi_S | \hat{H} | \psi_S \rangle - E_0 \leq \epsilon,$$

provided

$$\epsilon_{\text{prep}} = \mathcal{O}\left(\frac{(1 - e^{-2\tau\Delta}) \epsilon}{\|\hat{H}\|}\right).$$

Moreover, given a block-encoding of \hat{H}/α ($\alpha \geq \|\hat{H}\|$), the final energy $\langle \psi_S | \hat{H} | \psi_S \rangle$ can be estimated to additive error ϵ with failure probability at most δ using

$$\tilde{\mathcal{O}}(\alpha \epsilon^{-1} \log(1/\delta))$$

coherent uses of the final state-preparation routine together with the block-encoding [37].

Similar to standard analysis of numerical methods for differential equations, we organize the proof in three parts:

(i) one-segment local error, (ii) contraction under imaginary-time projection, and (iii) the recursion that yields the global error bound.

Local error. Write the normalized, ideal, one-segment imaginary-time map as

$$\Phi_\tau(\rho) := \frac{K_\tau \rho K_\tau}{\text{Tr}(K_\tau \rho K_\tau)}, \quad K_\tau := e^{-\tau(\hat{H} - E_T)}.$$

We used a Kraus form for the density matrix that is commonly used in expressing imaginary time evolution. Since E_T is a scalar, the normalized map Φ_τ is independent of the choice of shift. Thus the ideal state after S segments is

$$\rho_S^* = \Phi_\tau^S(\rho_0), \quad \rho_0 = |\psi_T\rangle\langle\psi_T|.$$

Meanwhile, one segment of our algorithm admits a coherent fault-tolerant approximation of the channel, denoted by $\tilde{\Phi}_\tau$. We choose the step size Δt , such that,

$$\sup_\rho \|\tilde{\Phi}_\tau(\rho) - \Phi_\tau(\rho)\|_1 \leq c_{\text{prep}} \epsilon_{\text{prep}}. \quad (\text{F2})$$

This bound is obtained from two contributions. First, the second-order Magnus truncation has local slice error $\mathcal{O}(\Delta t^3)$, hence over one segment

$$n_T \mathcal{O}(\Delta t^3) = \mathcal{O}(\tau \Delta t^2) = \mathcal{O}(\epsilon_{\text{prep}}),$$

using $\tau = \Theta(1/\|\Omega\|)$ and $\Delta t = \Theta(\sqrt{\epsilon_{\text{prep}}})$ (F1). Second, the dilation/LCU approximation is chosen so that the cumulative slice implementation error over one segment is also $\mathcal{O}(\epsilon_{\text{prep}})$, by using the light cone condition and increasing n_A . In the constant-success regime $\tau = \Theta(1/\|\Omega\|)$, oblivious amplitude amplification yields a coherent normalized segment routine, so (F2) holds uniformly in the input state.

Energy contraction. This is the same gap-overlap contraction mechanism that underlies fault-tolerant imaginary-time and spectral-filtering algorithms for ground-state preparation; see, e.g., Refs. [7, 8]. Let

$$P_0 = |E_0\rangle\langle E_0|, \quad g(\rho) := \text{Tr}(P_0 \rho), \quad r(\rho) := \frac{1 - g(\rho)}{g(\rho)}.$$

For the initial trial state $\rho_0 = |\psi_T\rangle\langle\psi_T|$, we have

$$g(\rho_0) = \gamma, \quad r(\rho_0) = \frac{1 - \gamma}{\gamma}.$$

More generally, if $\rho = \sum_{j,k} \rho_{jk} |E_j\rangle\langle E_k|$, then

$$g(\Phi_\tau(\rho)) = \frac{\rho_{00}}{\rho_{00} + \sum_{k \geq 1} \rho_{kk} e^{-2\tau(E_k - E_0)}},$$

and therefore

$$r(\Phi_\tau(\rho)) = \frac{\sum_{k \geq 1} \rho_{kk} e^{-2\tau(E_k - E_0)}}{\rho_{00}} \leq e^{-2\tau\Delta} r(\rho).$$

To proceed, we define

$$q := e^{-2\tau\Delta} \in (0, 1),$$

we obtain after S ideal segments

$$r(\rho_S^*) \leq q^S \frac{1 - \gamma}{\gamma}. \quad (\text{F3})$$

To convert this into an energy bound, set

$$C_H := \|\hat{H} - E_0 I\| \leq 2\|\hat{H}\|.$$

For any normalized ρ with $\rho = \sum_{j,k} \rho_{jk} |E_j\rangle\langle E_k|$, the following holds

$$\text{Tr}\left[(\hat{H} - E_0 I)\rho\right] = \sum_{k \geq 1} \rho_{kk} (E_k - E_0) \leq C_H \sum_{k \geq 1} \rho_{kk} = C_H (1 - g(\rho)).$$

Hence we have

$$\text{Tr}\left(\hat{H}\rho\right) - E_0 \leq C_H \frac{r(\rho)}{1 + r(\rho)} \leq C_H r(\rho).$$

Combining this with (F3) yields the ideal contraction estimate

$$\text{Tr}\left(\hat{H}\rho_S^*\right) - E_0 \leq C_H q^S \frac{1 - \gamma}{\gamma}. \quad (\text{F4})$$

Global error. Again let $\rho_{s+1} := \tilde{\Phi}_\tau(\rho_s)$ be the actually prepared state after $s + 1$ segments. Since the ideal map increases the ground weight and the segment error bound (F2) is uniform, all states ρ_s remain in a compact set with

$g(\rho_s)$ bounded below by a constant depending only on γ , provided ϵ_{prep} is sufficiently small. Thus, the map

$$g \mapsto r = \frac{1-g}{g}$$

can be made Lipschitz. Therefore there exists a constant $C_\gamma > 0$, depending only on the initial overlap γ , such that

$$r(\tilde{\Phi}_\tau(\rho)) \leq r(\Phi_\tau(\rho)) + C_\gamma \epsilon_{\text{prep}}$$

for every normalized input ρ .

Comparing to the ideal contraction from the previous step, we obtain the recursion

$$r(\rho_{s+1}) \leq q r(\rho_s) + C_\gamma \epsilon_{\text{prep}}.$$

Iterating gives

$$r(\rho_S) \leq q^S \frac{1-\gamma}{\gamma} + \frac{C_\gamma}{1-q} \epsilon_{\text{prep}}. \quad (\text{F5})$$

Applying again the energy bound $\text{Tr}(\hat{H}\rho) - E_0 \leq C_H r(\rho)$, we obtain

$$\langle \psi_S | \hat{H} | \psi_S \rangle - E_0 \leq C_H q^S \frac{1-\gamma}{\gamma} + \frac{C_H C_\gamma}{1-q} \epsilon_{\text{prep}}. \quad (\text{F6})$$

We now choose parameters so that each term in (F6) is at most $\epsilon/2$. For the contraction term, it suffices to take

$$S \geq \frac{1}{2\tau\Delta} \log\left(\frac{2C_H(1-\gamma)}{\gamma\epsilon}\right),$$

which implies

$$S = \Theta\left(\frac{\|\Omega\|}{\Delta} \log \frac{1}{\gamma\epsilon}\right) = \Theta(\kappa \log(1/(\gamma\epsilon)))$$

under $\tau = \Theta(1/\|\Omega\|)$. The logarithmic dependence on γ^{-1} here pertains only to the number of imaginary-time segments needed to contract the excited-state weight.

For the preparation error term, it suffices to require

$$\epsilon_{\text{prep}} \leq \frac{(1-q)\epsilon}{2C_H C_\gamma}, \quad q = e^{-2\tau\Delta},$$

which is equivalent to

$$\epsilon_{\text{prep}} = \mathcal{O}\left(\frac{(1 - e^{-2\tau\Delta})\epsilon}{\|\hat{H}\|}\right).$$

This proves the state-preparation part of the theorem. Finally, once the segment routine is available coherently, the full preparation of $|\psi_S\rangle$ is obtained by composing the S segment unitaries and their ancilla restorations. Given in addition a block-encoding of \hat{H}/α , standard coherent expectation-estimation primitives imply that $\langle \psi_S | \hat{H} | \psi_S \rangle$ can be estimated to additive error ϵ with failure probability at most δ using

$$\tilde{\mathcal{O}}\left(\alpha \epsilon^{-1} \log \frac{1}{\delta}\right)$$

controlled uses of the final state-preparation routine together with the block-encoding [37]. This proves the theorem.